PCCP

ROYAL SOCIETY OF CHEMISTRY

PAPER

View Article Online
View Journal | View Issue

Cite this: *Phys. Chem. Chem. Phys.*, 2020, **22**, 17705

Solvation and diffusion of poly(vinyl alcohol) chains in a hydrated inorganic ionic liquid†

Parvin Karimineghlani, [a] Jin Zheng,[b] Yan-Yan Hu[bc] and Svetlana Sukhishvili *[a]

While the behavior of polyelectrolyte chains in aqueous salt solutions has been extensively studied, little is known about polar polymer chains in solvents with extremely high concentrations of inorganic ions, such as those found in ionic liquids (ILs). Here, we report on expansion, solvation and diffusion of poly(vinyl alcohol), PVA, chains in dilute solutions of a hydrated inorganic IL phase change material (PCM), lithium nitrate trihydrate (LNH). This solvent has an extremely high concentration of inorganic ions (≈18 M) with a low concentration of water molecules largely forming solvation shells of Li^+ and NO_3^- ions, as shown using ATR-FTIR spectroscopy. Diffusion and hydrodynamic size of PVA chains of different molecular weights in this unusual solvent were studied using fluorescence correlation spectroscopy (FCS). A higher scaling exponent obtained from the molecular weight dependences of the diffusion coefficients of PVA chains as well as a lower overlap concentration (c^*) of PVA in LNH solutions as measured by FCS suggest an expansion of the polymer coils in this solvent. We argue that enhanced solubility of PVA in LNH solutions is likely a result of increased rigidification of polymer chains due to the binding of solvated Li^+ ions, which is demonstrated using ^{7}Li NMR spectroscopy. We believe that an understanding of solvation and ion-binding capability can offer crucial insight into designing polymer-based shape stabilization matrices for inorganic PCMs.

Received 17th May 2020,
Accepted 22nd July 2020

DOI: 10.1039/d0cp02679d

rsc.li/pccp

Introduction

Phase change materials (PCMs) possess the unique capability for absorbing/releasing large amounts of energy over a narrow temperature range associated with a phase transition and thus present promising and inexpensive solutions in thermal energy storage applications.[1] In comparison to widely used organic PCMs, such as paraffins, inorganic PCMs offer several unique properties, including nonflammability and high levels of thermal conductivity and volumetric latent heat capacity.[2,3] One specific representative of inorganic PCMs – lithium nitrate trihydrate (LNH) – is considered promising for energy storage applications because of its close-to-ambient melting temperature (≈30 °C) and high specific heat of fusion (≈290 J g^{-1}).[4] However, because of the high fluidity of LNH in its molten state (viscosity as low as 5.71 mPa s^{-1} at 30 °C), incorporation of this material within a shape-stabilizing matrix is required to efficiently harness its thermal storage properties. In our prior work, we have introduced poly(vinyl alcohol), PVA, gel matrices – called 'salogels' – as an efficient means to provide such shape stabilization, and then to remove and replace the used LNH after multiple heating/cooling cycles by a temperature-triggered dissolution of the salogel matrix.[5] We also explored the role of physical crosslinkers in gelation and studied the viscoelasticity of shape-stabilized salogels.[6,7] However, the factors that contribute to the gelation of PVA in LNH, as opposed to water remain unexplored.

In salt-free aqueous PVA solutions, polymer chains are solubilized, and no gelation occurs even at high polymer concentrations. Gelation can be induced, however, through inter- and intramolecular polymer–polymer hydrogen bonding between crystallized PVA domains that emerge as a result of freeze-thawing,[8] or can be mediated by multivalent organic[9] or inorganic salt ions, such as borate[10–12] or vanadate.[13] Binding of multivalent ions with polymer chains was identified as the main reason for gelation in moderate ion concentrations. An increase in ion concentration beyond a certain value (~40 mM for borax), however, resulted in the emergence of a strong charge on PVA chains, a significant decrease in the number of crosslinks, and suppressed gelation.[12]

[a] *Department of Materials Science and Engineering, Texas A&M University, College Station, 77843, TX, USA. E-mail: svetlana@tamu.edu; Fax: +979 862 6835; Tel: +979 458 9840*
[b] *Department of Chemistry & Biochemistry, Florida State University, Tallahassee, FL 32306, USA*
[c] *Center of Interdisciplinary Magnetic Resonance, National High Magnetic Field Laboratory, Tallahassee, FL 32310, USA*

† Electronic supplementary information (ESI) available: This file includes viscometry data used to determine the intrinsic viscosity, FCS calibration curves used to determine the diameter of the excitation beam, UV data to measure the degree of PVA labeling, and ^{7}Li NMR spectra of LNH and 15 wt% PVA–LNH solutions. See DOI: 10.1039/d0cp02679d

Gelation of PVA occurs much more readily when water is replaced with a different solvent – a hydrated inorganic ionic liquid (IL), which also is used as a PCM. Unlike common ILs which are composed entirely of ions, these new solvents are made of salt ions which are hydrated by water molecules supplied by the crystalline frameworks of the hydrates. Little is known, however, about behavior of polymer chains in hydrated inorganic ILs. In contrast, behavior of polymer coils in organic ILs has been considerably explored because of the relevance of these systems for applications in solar cells and lithium batteries.[14,15] Both experimental[16] and theoretical[17–19] studies emphasized significantly different interactions of polymer chains with organic ILs from those found in typical polymer solvents. In the case of poly(ethylene oxide) (PEO) solutions in imidazolium-based ILs, for example, enthalpically favorable and entropically unfavorable hydrogen bonding between oxygen and imidazolium-hydrogen of an IL were found to play a major role in expansion of PEO coils and the emergence of LCST behavior. Recent simulations predicted, for example, an expansion of PEO coils in an imidazolium-based IL with a mass scaling exponent of ~ 0.56.[20] Strong interactions between polymer units and ILs were also shown to affect the sol-to-gel transition of poly(*N*-isopropylacrylamide), PNIPAM,[21] as well as improve the thermal stability of PVA.[22] Experimentally, altering anion basicity and cation alkyl length of ILs (*e.g.* 1,3-dialkylimidazolium tetrafluoroborate) also had a significant impact on PEO coil dimensions.[14] In contrast to typical ILs, in which the polymer solvation can occur only through cation/anion interactions with polymer chains, hydrated inorganic ILs, always contain water in the amount incorporated in the crystalline lattice of the hydrates in their solid form. In the case of liquid LNH, water amounts for 3 molecules per 2 inorganic ions, and this solvent can be viewed as an aqueous solution with an extremely high ($\approx$18 M) concentration of inorganic ions. In such a solvent, water is scarce and largely utilized for solvation of ions, and polymer chains compete with salt ions for solvating water.

This work aims to understand the solvation of PVA chains in LNH solvent and compare it with what is observed in aqueous solutions. Polymer chain solvation and ion binding are important to understand physical gelation, in which polymer–polymer interactions are mediated by these parameters.[23] At the same time, solvation of polymer chains also influences excluded volume and hydrodynamic interactions within the polymer coil and thus affects the degree to which polymer chains are permeable to a solvent. The simplest model of polymer chains with strong hydrodynamic interactions was often used to interpret the results of hydrodynamic measurements in polymer solutions. Specifically, the scaling of hydrodynamic radius, diffusion coefficient, intrinsic viscosity and sedimentation coefficient with polymer molecular weight was used to evaluate solvent quality based on the value of the mass scaling exponents associated with these properties.[24–27] For polymer chains with increased excluded volume interactions, however, draining of polymer coils was theoretically predicted.[28–31] These models were further developed and experimentally tested for the case of rigid-chain polymers, such as DNA dissolved in water.[32] The effects of hydrated inorganic IL solvents on the hydrodynamics of polymer chains remain largely unexplored, however. In particular, it is unclear if the Flory exponents are the same for polymers having long range dipolar interactions and it is unclear how strong solvation might alter the strength of polymer–polymer hydrodynamic interactions. Here, we investigate the hydrodynamic solution properties of a polar flexible polymers in a hydrated inorganic IL to compare with the well-established phenomenology of neutral polymers in non-associating organic solvents.

Among experimental techniques capable of validating the earlier polymer diffusion models and relating them to chain solvation, fluorescence correlation spectroscopy (FCS) is one of the most suitable ones. This technique has an extremely high, single-molecule sensitivity that allows easy access to extremely dilute solutions, where chain diffusivity becomes concentration-independent.[33] At the same time, through using mixtures of fluorescently labeled and unlabeled polymer chains, FCS enables studies of chain motions in solutions at higher polymer concentrations. So far, applications of FCS to dilute aqueous polymer solutions generated sets of results that were consistent with the traditional model of non-draining polymer coils.[24,34,35] Here, we explore the diffusion of PVA chains and the overlap concentration (c^*) in a molten hydrated inorganic IL, LNH, and demonstrate strong chain solvation results. Finally, we show that enhanced solvation of the polar PVA polymer chains in LNH involves binding of Li^+ ions to polymer chains and suggest that such binding also contributes to the increased propensity of PVA to physical gelation in this solvent.

Experimental section

Materials

Anhydrous lithium nitrate (purity > 99%), butanol, dimethyl sulfoxide (DMSO) and triethylamine were purchased from Alfa Aesar and used as received. Four PVA samples with a hydrolysis degree of 99% were synthesized using a previously described procedure.[36] Gel permeation chromatography (GPC) traces for the PVA samples are shown in Fig. S1 (ESI†). The molecular weights and PDIs are shown in Table 1. Fluorescein isothiocyanate isomer I (FITC) and dibutyltin dilaurate were obtained from Sigma Aldrich and used without further purification.

LNH was prepared by mixing anhydrous lithium nitrate with stoichiometric amounts of deionized water. Polymer solutions in LNH were prepared by adding PVA to molten LNH, heating and stirring solutions at 80 °C for 6 h, followed by cooling to the ambient temperature. Aqueous solutions of PVA were prepared by heating and stirring at 90 °C for 24 h.

Table 1 Characteristics of PVA samples

Sample	M_w (g mol^{-1})	PDI
PVA1	29 500	1.2
PVA2	69 700	1.39
PVA3	107 000	1.62
PVA4	135 200	1.54

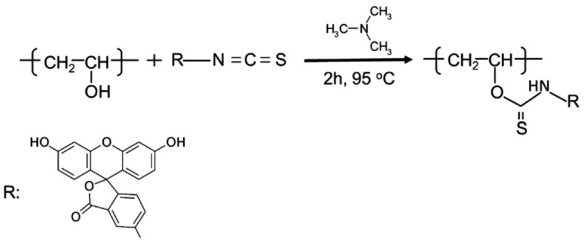

Scheme 1 PVA labeling reaction.

Fluorescent labeling of PVA. PVA was labeled with FITC by using the modified method of de Belder and Granath.[37] First, 150 mg of PVA were dissolved in 4 mL of DMSO by stirring and heating at 70 °C. Then, trimethylamine (25 μL), dibutyltin dilaurate (10 mg) and FITC (25 mg) were added consecutively to the polymer solution. The solution was stirred for 2 h at 95 °C to complete the reaction and purified from the unreacted dye by repeated precipitation in butanol, (Scheme 1). Fluorescently labeled PVA (PVA*) was then dried in the oven at 80 °C, dissolved in water and further purified from the unreacted FITC by extensive dialysis against water in a 5 L container for about a month. The water was refreshed daily during the first week, and then every 3 to 4 days. The external and internal solutions were periodically analyzed for the presence of free FITC, and the dialysis was terminated when no free fluorescent labels were detected in the internal or external solutions using FCS. The degree of labeling was determined by measuring the fluorescent intensities of 1 mg ml^{-1} PVA* aqueous solutions and comparing them against a calibration curve obtained with aqueous solutions of FITC of known concentrations (Fig. S2, ESI†). This analysis yielded the labeling degree of approximately one label per 45 monomer units for PVA* of all molecular weights.

Methods

Fluorescence correlation spectroscopy (FCS). FCS experiments were conducted using a custom-made setup which includes a World Star Tech laser, TECBL-488. A 488 nm beam was reflected from a mirror after filtering with Thorlabs NE10B and passing through an attenuator. Upon reflection, laser irradiated the back aperture of an Olympus 60× oil immersion objective, N.A. 1.45 to reach to the sample. The emission was collected after filtering with a Semlock 474/25 narrow-band filter and sent to an Excelitas SPCM-AQRH-14-FC photon detection counting module. A custom-made glass cell was used to hold sample solutions. Time fluctuations of intensity were collected for 30 minutes for each sample, and results were averaged over three repeated measurements. In FCS, diffusion coefficients of the fluorescently-labeled molecules are determined from the intensity correlation function (ICF), which is defined as:[38,39]

$$G(\tau) = \frac{\langle \delta I(t) \delta I(t+\tau) \rangle}{\langle I(t) \rangle^2} \quad (1)$$

where τ is the decay time, and $\delta I(t) = I(t) - \langle I \rangle_t$ where $\langle I \rangle_t$ is the time-averaged intensity.

In the case of translational diffusion of monodispersed fluorescent species, the ICF is related with the diffusion coefficient through the following equation:[40]

$$G(t) = \frac{1}{N}\left(1 + \frac{4Dt}{\omega_{xy}^2}\right)^{-1}\left(1 + \frac{4Dt}{\omega_z^2}\right)^{-1/2} \quad (2)$$

where ω_{xy} and ω_z are the radii of the laser excitation volume in xy and z directions, N is the average number of fluorescent particles in the excitation volume and D is the coefficient of transitional diffusion. Calibration of the FCS setup was performed by measuring the diffusion time of a fluorescent dye with known D. FITC dye with $D \sim 425$–490 μm^2 s^{-1} at 22 °C[41,42] for calibration gave a beam waist (ω_{xy}) of 0.323 μm (Fig. S3, ESI†).

Viscosity measurements. Viscosity measurements were carried out using a TA Instruments DHR-2 rheometer equipped with a double-gap geometry attachment. Water and LNH dynamic viscosities measured by this technique were 1.05 and 6.91 mPa s^{-1} at 22 °C, respectively.

Attenuated total reflection Fourier transform infrared spectroscopy (ATR-FTIR). A Nicolet 380 FTIR spectrometer with a single-reflection diamond ATR was used to perform ATR-FTIR measurements. A drop of a molten salt hydrate was carefully put on the crystal to measure the corresponding spectrum. In order to eliminate the overlap of the –OH stretching vibrations bands of PVA and water, D_2O was used instead of H_2O for FTIR measurements. The spectra were collected at a 4 cm^{-1} resolution using 64 scans. Deconvolution was performed by Origin 8.5 software assuming Gaussian band shapes and keeping peak positions fixed at the values which were previously reported in the literature.[43–45]

^{7}Li nuclear magnetic resonance (NMR) spectroscopy. ^{7}Li NMR experiments were acquired at room temperature (22 °C) on a Bruker Avance III spectrometer at a field of 11.7 T with the ^{7}Li Larmor frequency of 194.4 MHz. The 90° pulse length was 2 μs. The recycling delay was 10 s. ^{7}Li chemical shift was referenced to 1 M LiCl at 0 ppm. Spectra were processed and analyzed using Topspin 4.0.5.

Results and discussion

Fig. 1 illustrates the effect of a solvent (LNH *vs.* water) on gelation and rheology of PVA solutions. While gelation occurred

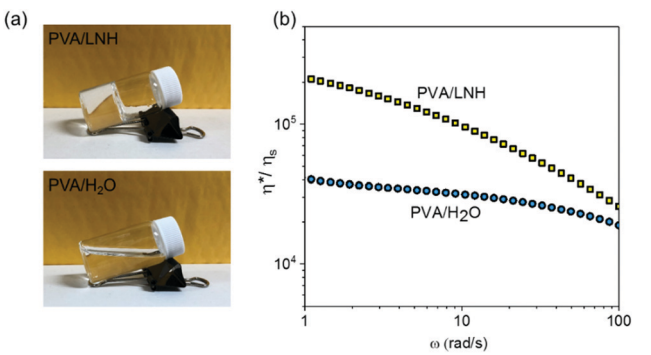

Fig. 1 Digital images (a) and frequency dependence of the relative shear viscosities (b) of 15% PVA3 solutions in LNH and water at T = 22 °C.

in 15 wt% PVA3 (M_w = 107 000 g mol^{-1}) solutions in LNH, aqueous solutions with the same concentration of the polymer had a significantly lower viscosity and easily flowed (Fig. 1a).[5] Fig. 1b shows that while the relative viscosity of aqueous PVA solutions was weakly dependent on the shear rate – a behavior close to that of a Newtonian fluid – the gelled samples exhibited strong shear-thinning behavior, typical of associating liquids. Note that LNH did not crystallize at room temperature due to the supercooling effect, enanbling us to use it as a solvent without rising the temperature.[4]

Physical gelation in polymer solutions is often related to poor solvation of polymer chains at the crosslink points, such as, for example, the association between PVA chains induced by freeze-thawing.[46] However, polymers of all molecular weights studied here were readily soluble in LNH. Specifically, shorter stirring times and lower temperatures were needed to prepare PVA solutions in LNH as compared to water (see Experimental section). To understand the nature of the gelation of PVA in LNH, we aimed to study the intricate details of the solvation of PVA chains and their interactions with the abundant LNH ionic species.

Molten LNH salt is an unusual solvent, which presents an $\approx$18 M aqueous solution of lithium nitrate salt. When compared to typical ILs,[47] LNH is unique in its role as a high-heat-capacity PCM. Water molecules in the high-salt environment of LNH are scarce and extensively used to solvate Li^+ and NO_3^- ions. In such a solvent, the effects of ion solvation on the solution properties – an effect only recently been developed theoretically for other systems[48] – should be especially strong. The intricate solvation structure of the LNH can be revealed through FTIR analysis of vibrational bands associated with different types of noncovalent intermolecular bonding.

In the ATR-FTIR spectroscopy studies, replacing H_2O with D_2O has enabled us to avoid the overlap of –OH vibrational bands originating from PVA and LNH. Specifically, the use of fully deuterated lithium nitrate (LND) and D_2O enabled the selective observation of –OD stretching vibrations in the 2000–2800 cm^{-1} region. The 3000–3300 cm^{-1} –OH stretching region was examined in our previous paper, and a significant blue shift in the –OH vibrational frequencies of PVA was observed upon increasing salt concentration in aqueous solutions.[5] This change indicated a weakening of hydrogen bonding between –OH groups of PVA and water when the concentration of salt ions was increased. We hypothesize here that lower hydration of PVA results from strong binding of water within the solvation shell of Li^+ and NO_3^- ions. Similarly, lower hydration of PVA and chitosan was also reported for typical ILs, which can bind with water stronger than with polymer units.[49,50] To better understand the binding of water with salt ions in LNH, we focused here on the –OD stretching (2000–2800 cm^{-1}) vibration region which is sensitive to hydrogen bonding and structure formation in heavy water.

Fig. 2 shows that dramatic changes occurred in the overall peak shape in the –OD stretching vibrational region as D_2O was gradually replaced with LND. Mixed solutions are abbreviated as D_2O/LND (x/y), where x/y is the volume ratio of D_2O to LND. In water, there exist a broad range of water–water hydrogen-bonded configurations that vary in both their energy and the binding angle between the donor (D) and acceptor (A) moieties of water molecules, but all can be grouped within two main types of weakly and strongly hydrogen-bonded water.[51,52] In this work, we based the deconvolution procedure on the theoretical prediction of the existence of two additional sub-peaks of strongly and weakly hydrogen-bonded water.[43,53] The peaks centered at 2336 cm^{-1}, 2383 cm^{-1}, 2493 cm^{-1}, 2580 cm^{-1}, and 2648 cm^{-1} are assigned to –OD vibrations involved in the strongest DAA (single donor and double acceptor, symmetric stretching vibration) hydrogen-bonding, strong DDAA (double donor – double acceptor, symmetric stretching vibration) tetrahedral hydrogen bonding, weak DA (single donor–single acceptor, bending vibration) and another weak DDA (double donor–single acceptor, antisymmetric stretching vibration) hydrogen bonds, as well as to stretching vibrations of free –OD groups, respectively. For D_2O, the wavenumbers of the contributing deconvoluted bands and their intensities were consistent with prior theoretical and experimental results.[43–45] Deconvolution of the absorbance bands (see Experimental section for details) revealed significant changes in both positions and relative intensities of the contributing –OD bands. With increasing salt concentration, the positions of all peaks shifted to higher wavenumbers (Fig. 2b), suggesting a weakening of water–water hydrogen bonding in solutions with high concentrations of Li^+ and NO_3^- ions. At the same time, the fractional intensities of weaker H-bonds (DA and DDA) increased at the expense of intensities of the stronger DAA and DDAA hydrogen bonds (Fig. 2c). These results suggest that Li^+ and NO_3^- ions drastically changed the energy and structure of hydrogen-bonding networks of water molecules in the aqueous environment. Strong competition of inorganic ions and water–water hydrogen bonding occurred because of the scarcity of water in LNH, with only three water molecules being available for a pair of Li^+–NO_3^- ions. The data in Fig. 2, therefore, illustrate breaking of the water–water hydrogen bonds which are abundant in salt-free water and emergence of weaker hydrogen-bonded water, which is included in solvation shells of Li^+ and NO_3^- ions.

Weaker hydration of PVA chains, resulting from competition for water between the polymer chains and LNH, reduced the number of hydrogen bonds between –OH groups of PVA and water. One can suggest that this could facilitate the formation of polymer–polymer hydrogen bonding and thus contributing to gelation. Alternatively, gelation can be mediated through the binding of solvated inorganic ions. Li^+ ions are known to coordinate with high-electron-density species, such as sulfur or oxygen atoms;[54,55] thus we hypothesized that Li^+ ions can bind with –OH groups of PVA. To test this hypothesis, we have performed ^{7}Li NMR studies of the mobility of Li^+ ions in PVA-free and PVA-containing LNH solutions.

^{7}Li NMR spectra of LNH and PVA3/LNH solutions are displayed in Fig. S4 (ESI†). The ^{7}Li NMR resonance of PVA3/LNH is significantly broadened compared to polymer-free LNH, owing to the reduced Li^+ ion mobility in the viscous PVA3 polymer matrix. To further investigate the effects of PVA on Li^+ ion mobility, we performed ^{7}Li NMR spin–lattice relaxation

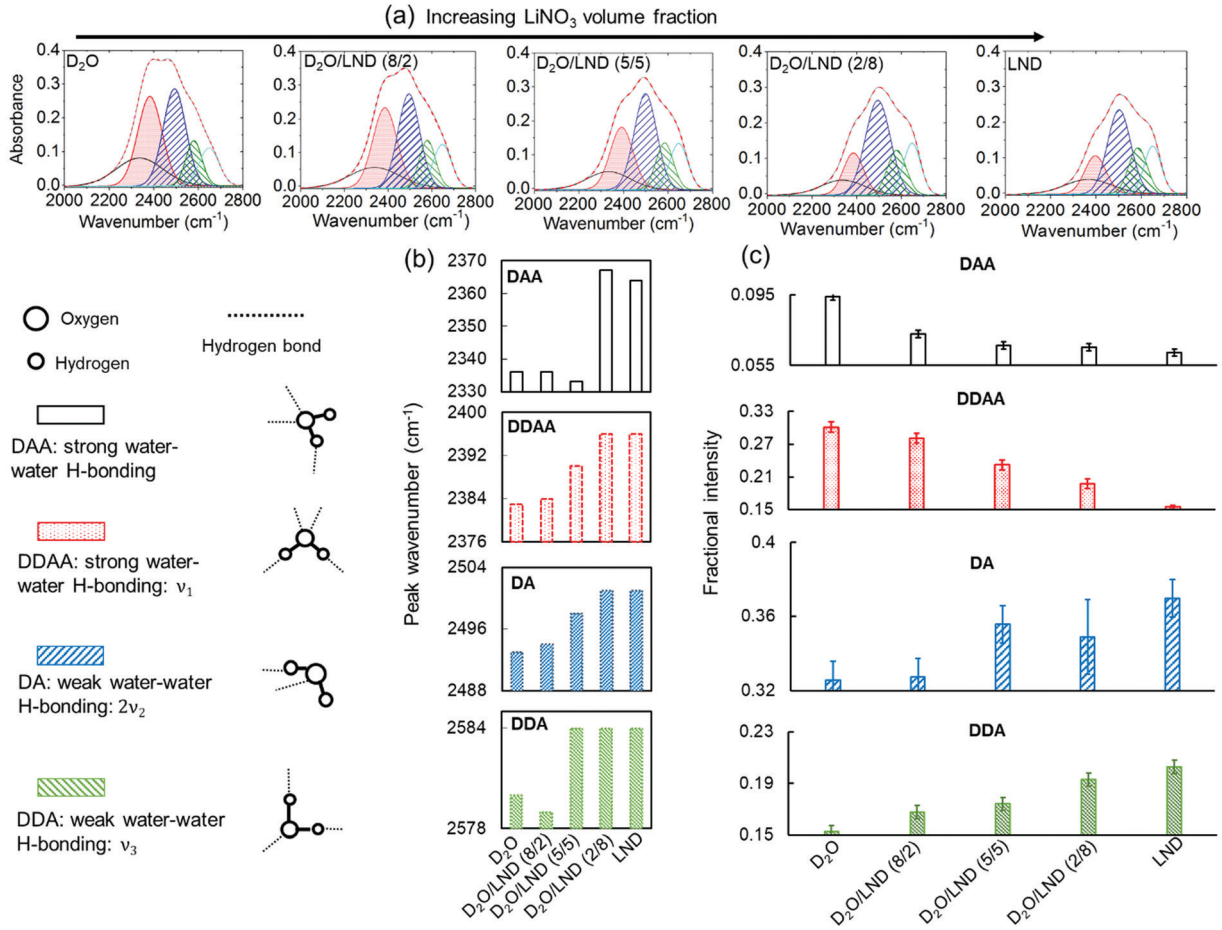

Fig. 2 FTIR analysis of 2000–2800 cm^{-1} –OD vibrational region in LND, D_2O, and D_2O/LND mixed solvents (a), peak wavenumber (b) and fractional intensity (c) changes corresponding to the deconvoluted peaks of DAA, DDAA, DA, and DDA vibrations upon gradual transition from D_2O to LND.

time (T_1) measurements which provide important clues in ion dynamics.[56] Fig. 3 shows that the initial ^{7}Li NMR T_1 in LNH of 3.6 s gradually decreases upon addition of PVA, reaching a value of 1.2 s in 15% PVA3/LNH solution. Spin–lattice relaxation is generally described by the Bloembergen, Purcell, and Pound (BPP) model:[57]

$$\frac{1}{T_1} \propto \frac{\tau_c}{1 + (\omega_0 \tau_c)^2} \quad (3)$$

where τ_c is the correlation time and ω_0 is the Larmor frequency.

For smaller molecules at room temperature, such as LNH, ion dynamics falls in the fast-motion region, where $\omega_0\tau_c \ll 1$. Under these conditions, a decrease in T_1 indicates slowing down of ionic motions,[58] which in our system most likely occurred due to increased interactions between Li^+ ion and PVA chains.

After demonstrating strong solvation of inorganic ions in LNH and binding of Li^+ ions with PVA, we sought to explore the effect of these interactions on hydrodynamic properties of the polymer coils. To that end, we employed the FCS technique that is capable of probing polymer dynamics with single-molecule sensitivity (see Experimental section for details). Using fluorescently tagged PVA* chains of four different molecular weights with relatively narrow molecular weight distributions (Table 1), we first explored hydrodynamic properties of PVA coils in the dilute regime using LNH and water as solvents. In the dilute regime, polymer chains do not overlap, and hydrodynamic

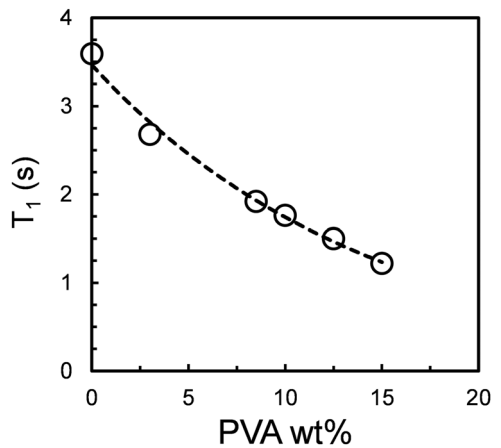

Fig. 3 ^{7}Li spin–lattice relaxation time (T_1) as a function of PVA3 concentration in LNH measured at 22 °C.

radius (R_H) of the polymer coils can be determined using the Stokes–Einstein equation, $D = k_BT/6\pi\eta R_H$. This equation applies regardless of the strength of the hydrodynamic interactions, but the "non-draining" limit of strong hydrodynamic polymer–polymer interactions mediated by the solvent is often assumed.

Fig. 4 shows the diffusion coefficients (D) of PVA* as a function of polymer molecular weight. Representative intensity correlation functions (ICFs) for the diffusion of PVA4* in aqueous and LNH solutions are shown in Fig. S5 (ESI†). For flexible chains in theta and good solvents, diffusion coefficients for non-draining polymer coils are expected to scale as $D \sim M^{-1/2}$ and $D \sim M^{-3/5}$, respectively.[59,60] Here, for solutions of PVA* in LNH and water, the diffusion mass scaling exponents were 0.6 ± 0.1 and 0.45 ± 0.10, respectively (Fig. 4). This result is in a good agreement with the scaling exponents of PEO in IL of 1-butyl-3-methylimidazolium tetrafluoroborate ($BMIM^+BF4^-$) and water which reported to be 0.56[20] and 0.5,[18] respectively. However, no strong conclusions regarding solvent quality can be made here, considering the relatively narrow range of molecular weights, moderate polydispersity of the samples, and the experimental error of the measurements. Prior publications by others have also advised caution in interpreting the mass scaling exponents as direct measures of the equilibrium size of polymer chains in solution.[14]

An attempt to re-calculate hydrodynamic radii (R_H) of PVA* chains using the Stokes–Einstein equation, $D = k_BT/6\pi\eta R_H$ is shown in Fig. S6 (ESI†). The hydrodynamic sizes in aqueous PVA* solutions agreed well with prior reports and can be interpreted using the non-draining polymer coil model.[61] However, hydrodynamic radii of PVA* chains in LNH were lower as compared to those in water, which were consistently observed for polymers of all molecular weights. The smaller hydrodynamic diameters of the polymer chains in the PVA/LNH system were also confirmed by the measurements of intrinsic viscosity with 2 to 10 mg ml^{-1} PVA solutions (Fig. S7, ESI†). These concentrations fell within the dilute solution regime (Fig. S8, ESI†), considering that c^* of 17.3 mg ml^{-1} was reported for PVA for the molecular weight of 166 000 g mol^{-1},[8] which is higher than all the molecular weights of PVA studied here (see Table 1). One explanation for a smaller hydrodynamic sizes of PVA chains in LNH could indicate partial collapse of the polymer coils in a solvent, but this explanation is inconsistent with the high exponents in the molecular mass dependences of D, R_H and intrinsic viscosity of PVA in LNH (Fig. 4 and Fig. S6, S7, ESI†). The results can be also lightly interpreted as an indication of draining of polymer coils in LNH solvent. A possibility of draining of polymer coils was already taken into account in earlier models by Flory[62] and Kirkwood and Riseman[63] and suggested by experiments performed with rigid chains in a good solvent.[32,64–66] More recently, Mansfield *et al.* performed hydrodynamic modeling of duplex DNA and found evidence of weak hydrodynamic interactions and significant draining of DNA coils for this semi-flexible polymer.[32] While DNA molecules are highly charged, the measurements described here are performed for polymer chains in a solvent with extremely high salt concentrations for which the charge interactions have been largely neutralized. It is also likely that hydrodynamic radius of polymer coils cannot be determined in highly charged inorganic ILs using the Stocks–Einstein equation or intrinsic viscosity measurements, due to strongly correlated ion motions in these solvents – an argument similar to that previously made for typical ILs.[67]

Finally, assessing the chain overlap concentration value c^* in these two solvents and comparing these values with mass scaling exponents measurements can provide another piece of evidence related to the solvent quality for polymer chains. The value of c^* separates the dilute and semidilute solution regimes of polymer solutions and indicates the onset of the physical overlap of the polymer coils determined by their R_g. The transition can be probed by measuring polymer dynamics in a wide range of solution concentrations. When polymer concentrations exceed c^*, chain diffusivity is slowed by the surrounding molecules.[33] In this work, this transition was explored by FCS measurements of diffusion of PVA* chains in solutions containing increasing concentrations of unlabeled PVA molecules. These experiments were performed using PVA2 with the average molecular weight M_w of 69 700 g mol^{-1} and polydispersity of 1.39.

Fig. 5a and c show the representative fluorescence intensity correlation functions and diffusion coefficients of PVA* added in an ultra-low amount to solutions of unlabeled PVA. An obvious shift of ICFs for diffusing PVA* to longer diffusion times was observed at higher concentrations of unlabeled PVA. Fig. 5b and d compares the results for PVA* diffusion in a wide range of PVA concentrations for the two solvents. The region of a nearly constant D at low polymer concentrations is followed by a strong decrease in PVA* mobility above the overlap concentration c^*. In the dilute regime ($c \ll c^*$), diffusion coefficients are expected to be independent on polymer concentration because of the separation of individual polymer coils.[60,68] Above the overlap concentration, the scaling of D *vs.* $c^{-1/2}$ was predicted for $c^* < c < c_e$ (the Rouse-like regime),[69] where c_e is the entanglement transition concentration. The data in Fig. 5b and d yielded the scaling exponents of 0.55 ± 0.15 and 0.7 ± 0.1 above the overlap concentration for water and LNH, respectively. Most importantly, the PVA chain overlap occurred at a twice higher concentration in water as

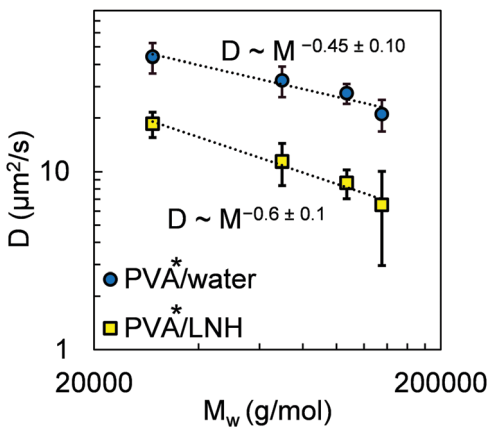

Fig. 4 Molecular weight dependences of FCS diffusion coefficients of PVA* measured in 10^{-4} mg ml^{-1} aqueous or LNH solutions at 22 °C.

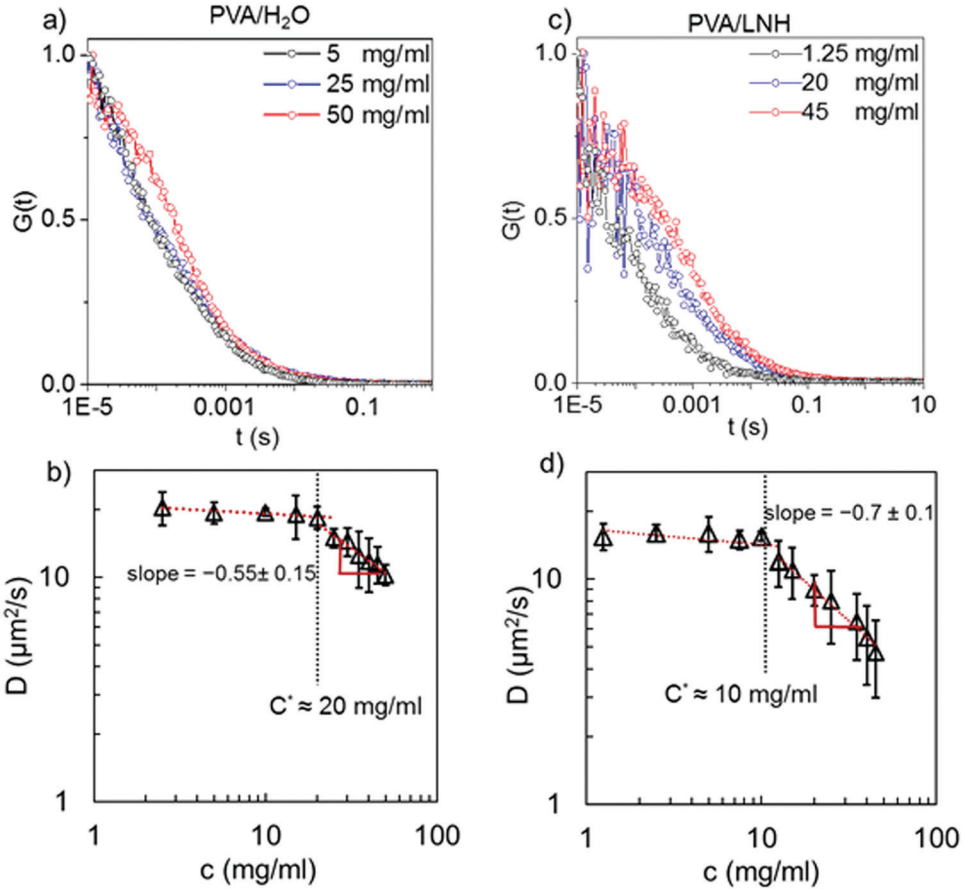

Fig. 5 FCS autocorrelation functions and diffusion coefficients in 10^{-4} mg ml^{-1} PVA2* solutions in water (a and b) and LNH (c and d), which also contained increasing amounts of unlabeled PVA2 with M_w of 69 000 g mol^{-1}. Temperature was 22 °C.

compared to LNH (20 *vs.* 10 mg ml^{-1}, respectively), suggesting ~25% larger radial and ~ two-fold volume chain expansion of PVA in LNH solvent. Taken together with the higher mass scaling values discussed above in the paper, the extension of physical chain dimensions of PVA in LNH, as shown by a decrease in c^*, as compared to water are suggestive of the overall a better solubility of PVA chains in LNH in comparison to water.

In summary, here we explored the behavior of a neutral polar polymer in a hydrated inorganic IL, LNH, and found that binding of components of this solvent with PVA chains led to increased chain rigidification and decreased hydrodynamic interaction strength, resulting in a better solvent quality for the polymer chains. The intricate details of interactions of ions and water molecules with hydrophilic polymer chains in the water-scarce environment of LNH raise new fundamental questions about the role of competitive hydration of polymers in ion-rich solutions. At the same time, these studies shed light on the mechanism of gelation of polymers in the highly ionic environments of LNH – a high-performance inorganic PCM whose applications demand controlled and efficient shape stabilization. We believe that an understanding of expansion and solvation of polymer chains in hydrated inorganic ILs can facilitate the development of new types of shape-stabilizing salogels for thermal storage applications.

Conflicts of interest

There are no conflicts to declare.

Acknowledgements

This work was supported by TEES at Texas A&M University and in part by the NSF under Award DMR-0906474. We thank Jack Douglas (National Institute of Standards and Technology) for insightful discussion and edits. We also thank Yuhao Wang from Stevens Institute of Technology for his help with labeling experiments.

References

1 D. Zhou, C.-Y. Zhao and Y. Tian, *Appl. Energy*, 2012, **92**, 593–605.
2 S. A. Mohamed, F. A. Al-Sulaiman, N. I. Ibrahim, M. H. Zahir, A. Al-Ahmed, R. Saidur, B. Yılbaş and A. Sahin, *Renewable Sustainable Energy Rev.*, 2017, **70**, 1072–1089.
3 N. Kumar, J. Hirschey, T. J. LaClair, K. R. Gluesenkamp and S. Graham, *J. Energy Storage*, 2019, **24**, 100794.
4 P. J. Shamberger and T. Reid, *J. Chem. Eng. Data*, 2012, **57**, 1404–1411.
5 P. Karimineghlani, E. Emmons, M. J. Green, P. Shamberger and S. A. Sukhishvili, *J. Mater. Chem. A*, 2017, **5**, 12474–12482.

6 P. Karimineghlani, A. Palanisamy and S. A. Sukhishvili, *ACS Appl. Mater. Interfaces*, 2018, **10**, 14786–14795.
7 P. Karimineghlani and S. A. Sukhishvili, *Macromol. Chem. Phys.*, 2019, **220**, 1900329.
8 M. Bercea, S. Morariu and D. Rusu, *Soft Matter*, 2013, **9**, 1244–1253.
9 M. Tsujimoto and M. Shibayama, *Macromolecules*, 2002, **35**, 1342–1347.
10 L. Gao, G. Guo, M. Liu, Z. Tang, L. Xie and Y. Huo, *RSC Adv.*, 2017, **7**, 40005–40014.
11 H. Ochiai, Y. Kurita and I. Murakami, *Macromol. Chem. Phys.*, 1984, **185**, 167–172.
12 J. Li, Z. Zhang, X. Cao, Y. Liu and Q. Chen, *Soft Matter*, 2018, **14**, 6767–6773.
13 M. Shibayama, M. Adachi, F. Ikkai, H. Kurokawa, S. Sakurai and S. Nomura, *Macromolecules*, 1993, **26**, 623–627.
14 A. Kharel and T. P. Lodge, *Macromolecules*, 2019, **52**, 3123–3130.
15 H.-N. Lee and T. P. Lodge, *J. Phys. Chem. Lett.*, 2010, **1**, 1962–1966.
16 H.-N. Lee, N. Newell, Z. Bai and T. P. Lodge, *Macromolecules*, 2012, **45**, 3627–3633.
17 E. Choi and A. Yethiraj, *ACS Macro Lett.*, 2015, **4**, 799–803.
18 J. Mondal, E. Choi and A. Yethiraj, *Macromolecules*, 2014, **47**, 438–446.
19 J. G. McDaniel, E. Choi, C.-Y. Son, J. Schmidt and A. Yethiraj, *J. Phys. Chem. B*, 2016, **120**, 231–243.
20 C. Y. Son, J. G. McDaniel, Q. Cui and A. Yethiraj, *Macromolecules*, 2018, **51**, 5336–5345.
21 Z. Wang and P. Wu, *J. Phys. Chem. B*, 2011, **115**, 10604–10614.
22 G. Chen, N. Chen, L. Li, Q. Wang and W. Duan, *Ind. Eng. Chem. Res.*, 2018, **57**, 5472–5481.
23 A. Chremos and J. F. Douglas, *Gels*, 2018, **4**, 20.
24 U. Zettl, S. T. Hoffmann, F. Koberling, G. Krausch, J. R. Enderlein, L. Harnau and M. Ballauff, *Macromolecules*, 2009, **42**, 9537–9547.
25 G. D. Phillies, *Macromolecules*, 1990, **23**, 2742–2748.
26 P. Zhou and W. Brown, *Macromolecules*, 1990, **23**, 1131–1139.
27 C. Chamignon, D. Duret, M. T. Charreyre and A. Favier, *Macromol. Chem. Phys.*, 2016, **217**, 2286–2293.
28 J. F. Douglas and K. F. Freed, *Macromolecules*, 1984, **17**, 2354–2364.
29 J. F. Douglas and K. F. Freed, *Macromolecules*, 1994, **27**, 6088–6099.
30 S. Q. Wang, J. F. Douglas and K. F. Freed, *J. Chem. Phys.*, 1987, **87**, 1346–1354.
31 M. L. Mansfield and J. F. Douglas, *Phys. Rev. E: Stat., Nonlinear, Soft Matter Phys.*, 2010, **81**, 021803.
32 M. L. Mansfield, A. Tsortos and J. F. Douglas, *J. Chem. Phys.*, 2015, **143**, 124903.
33 R. Liu, X. Gao, J. Adams and W. Oppermann, *Macromolecules*, 2005, **38**, 8845–8849.
34 S. A. Sukhishvili, Y. Chen, J. D. Müller, E. Gratton, K. S. Schweizer and S. Granick, *Macromolecules*, 2002, **35**, 1776–1784.
35 H. Zettl, U. Zettl, G. Krausch, J. Enderlein and M. Ballauff, *Phys. Rev. E: Stat., Nonlinear, Soft Matter Phys.*, 2007, **75**, 061804.
36 A. Debuigne, C. Detrembleur, R. Bryaskova, J.-R. Caille and R. Jérôme, Controlled/Living Radical Polymerization: From Synthesis to Materials, *ACS Symposium Series 944*, American Chemical Society, Washington, DC, 2006.
37 A. N. de Belder and K. Granath, *Carbohydr. Res.*, 1973, **30**, 375–378.
38 S. T. Hess and W. W. Webb, *Biophys. J.*, 2002, **83**, 2300–2317.
39 O. Krichevsky and G. Bonnet, *Rep. Prog. Phys.*, 2002, **65**, 251.
40 S. Aragon and R. Pecora, *J. Chem. Phys.*, 1976, **64**, 1791–1803.
41 S. A. Rani, B. Pitts and P. S. Stewart, *Antimicrob. Agents Chemother.*, 2005, **49**, 728–732.
42 C. T. Culbertson, S. C. Jacobson and J. Michael Ramsey, *Talanta*, 2002, **56**, 365–373.
43 Q. Sun and Y. Guo, *J. Mol. Liq.*, 2016, **213**, 28–32.
44 C. Choe, J. Lademann and M. E. Darvin, *Analyst*, 2016, **141**, 6329–6337.
45 J.-J. Max, P. Larouche and C. Chapados, *J. Mol. Struct.*, 2017, **1149**, 457–472.
46 C. M. Hassan and N. A. Peppas, *Macromolecules*, 2000, **33**, 2472–2479.
47 R. D. Rogers and K. R. Seddon, *Science*, 2003, **302**, 792–793.
48 M. Andreev, J. J. de Pablo, A. Chremos and J. F. Douglas, *J. Phys. Chem. B*, 2018, **122**, 4029–4034.
49 S. Paţachia, C. Friedrich, C. Florea and C. Croitoru, *eXPRESS Polym. Lett.*, 2011, **5**(2), 197–207.
50 G. M. Spinks, C. K. Lee, G. G. Wallace, S. I. Kim and S. J. Kim, *Langmuir*, 2006, **22**, 9375–9379.
51 J. B. Schlenoff, A. H. Rmaile and C. B. Bucur, *J. Am. Chem. Soc.*, 2008, **130**, 13589–13597.
52 P. Wernet, D. Nordlund, U. Bergmann, M. Cavalleri, M. Odelius, H. Ogasawara, L.-Å. Näslund, T. Hirsch, L. Ojamäe and P. Glatzel, *Science*, 2004, **304**, 995–999.
53 Q. Sun, *Vib. Spectrosc.*, 2009, **51**, 213–217.
54 K. D. Fong, J. Self, K. M. Diederichsen, B. M. Wood, B. D. McCloskey and K. A. Persson, *ACS Cent. Sci.*, 2019, **5**, 1250–1260.
55 R. Ganguly and V. Aswal, *J. Phys. Chem. B*, 2008, **112**, 7726–7731.
56 I. Hanghofer, M. Brinek, S. Eisbacher, B. Bitschnau, M. Volck, V. Hennige, I. Hanzu, D. Rettenwander and H. Wilkening, *Phys. Chem. Chem. Phys.*, 2019, **21**, 8489–8507.
57 N. Bloembergen, E. M. Purcell and R. V. Pound, *Phys. Rev.*, 1948, **73**, 679.
58 J. Adebahr, M. Forsyth, D. R. Macfarlane, P. Gavelin and P. Jacobsson, *J. Mater. Chem.*, 2003, **13**, 814–817.
59 P. J. Flory, *Principles of polymer chemistry*, Cornell University Press, 1953.
60 P.-G. De Gennes and P.-G. Gennes, *Scaling concepts in polymer physics*, Cornell university press, 1979.
61 B. Budhlall, K. Landfester, E. Sudol, V. Dimonie, A. Klein and M. El-Aasser, *Macromolecules*, 2003, **36**, 9477–9484.
62 P. Flory and W. Krigbaum, *J. Chem. Phys.*, 1950, **18**, 1086–1094.
63 J. G. Kirkwood and J. Riseman, *J. Chem. Phys.*, 1948, **16**, 565–573.
64 A. Dondos, *Phys. B*, 2010, **405**, 3572–3575.
65 A. Dondos, *Polym. Bull.*, 2011, **67**, 333–342.
66 D. Woodley, C. Dam, H. Lam, M. LeCave, K. Devanand and J. Selser, *Macromolecules*, 1992, **25**, 5283–5286.
67 T. Köddermann, R. Ludwig and D. Paschek, *ChemPhysChem*, 2008, **9**, 1851–1858.
68 T. Lodge, N. Rotstein and S. Prager, *Adv. Chem. Phys.*, 1992, **79**, 1.
69 P. De Gennes, *Macromolecules*, 1976, **9**, 587–593.

